

# Numerical estimation of structure constants in the three-dimensional Ising conformal field theory through Markov chain uv sampler

Victor Herdeiro

*Department of Mathematics, King's College, London WC2R 2LS, United Kingdom*

(Received 6 June 2017; published 5 September 2017)

Herdeiro and Doyon [*Phys. Rev. E* **94**, 043322 (2016)] introduced a numerical recipe, dubbed uv sampler, offering precise estimations of the conformal field theory (CFT) data of the planar two-dimensional (2D) critical Ising model. It made use of scale invariance emerging at the critical point in order to sample finite sublattice marginals of the infinite plane Gibbs measure of the model by producing holographic boundary distributions. The main ingredient of the Markov chain Monte Carlo sampler is the invariance under dilation. This paper presents a generalization to higher dimensions with the critical 3D Ising model. This leads to numerical estimations of a subset of the CFT data—scaling weights and structure constants—through fitting of measured correlation functions. The results are shown to agree with the recent most precise estimations from numerical bootstrap methods [Kos, Poland, Simmons-Duffin, and Vichi, *J. High Energy Phys.* **08** (2016) 036].

DOI: [10.1103/PhysRevE.96.033301](https://doi.org/10.1103/PhysRevE.96.033301)

## I. INTRODUCTION

*3D Ising model.* The Ising model is a milestone of statistical physics. It consists of a statistical model on a graph with binary random variables and nearest-neighbor interactions. Having been studied for more than a century now, it has given a lot of insight in the fields of materials physics and critical phenomena, among others.

One of its strengths lies in its easiness to be generalized to any dimensions or even fractal graphs. Peierls's argument [1] brought a satisfying qualitative proof of the existence of a critical point for the two-dimensional (2D) case. The generalization of his droplets to higher dimensions implied that such ordered-disordered phase transition had to exist for any dimension  $d \geq 2$ . For  $d = 2$ , the model has since been solved exactly by Onsager [2]; while for  $d \geq 4$  it has been proven that the Landau-Ginzburg theory gives the exact value of the critical exponents [3]. Only  $d = 3$  has resisted every attempt at an exhaustive solution so far.

Recent breakthroughs by means of the conformal bootstrap program applied to 3D conformal field theories (CFTs), e.g., the constraints of associativity and positivity on the CFT operator algebra, have led to the most precise estimation of the critical exponents and some structure constants [4–8]. The numerical precision of this approach has far overtaken previous Monte Carlo or analytical expansion results.

The goal of this paper is to extend the numerical procedure of Ref. [9] to the 3D Ising model. This numerical procedure, dubbed uv sampler, is a Markov chain Monte Carlo (MCMC) allowing us to sample sublattice marginals of infinite-volume statistical models at criticality by effectively producing a holographic boundary condition that encodes the infinite volume beyond it. It thus gives access directly to bulk data of the critical point, without the need for finite-size scaling. Catching up on the high precision of the bootstrap method seems out of reach of the numerical procedure introduced here, thus the aim is more of presenting an alternative approach using this MCMC and free of the bootstrap's assumptions. Its results will be shown to agree with the state-of-the-art knowledge on the 3D Ising universality class, giving a precision improvement of the Monte Carlo estimations of the structure constants ( $C_{\varepsilon\sigma\sigma}$ ,  $C_{\varepsilon\varepsilon\varepsilon}$ ) in this model.

*Markov chain holographic sampling.* Reference [9] studied the planar critical 2D Ising model through a MCMC. It showed that an implementation of dilations on a lattice statistical model at criticality coupled with a sufficiently long rethermalization step through fixed boundaries Swendsen-Wang (SW) lattice flip updates [10] would eventually mix into a Markov chain sampling the distribution of the sublattice marginal in the infinite plane Gibbs measure. Reference [11] showed a successful generalization of this method and its results to the  $O(1 < n \leq 2)$  loop gas models where nonlocal contributions have to be accounted for.

Let us recall the main arguments of Ref. [9]. Working on the complex plane with a radially quantized generic (Euclidean) CFT and picking  $A$  a disk centered on the origin, the subdomain marginal  $\Psi_{\partial A}$  is defined by

$$\Psi_{\partial A} = \int \mathcal{D}\phi_{\mathbb{C} \setminus A} e^{-S_{\mathbb{C} \setminus A}[\phi]}. \quad (1)$$

This can be enhanced to include operator insertions in  $\mathbb{C} \setminus A$ . Knowledge of  $\Psi_{\partial A}$  allows us to measure any infinite plane correlators with any insertions  $O_1(x_1)O_2(x_2)\dots O_n(x_n)$  as long as  $x_1, x_2, \dots, x_n \in A$ . In this sense it is the bulk marginal of  $A$ . An interesting observation is that the information on the marginal distribution is entirely contained on  $\partial A$  because of the ultralocality of the measure. In this respect it is holographic: it is a probability distribution on the set of boundary states of  $A$ , which reproduces, from the viewpoint of observables in  $A$ , the statistical information outside  $A$ . The goal of the uv sampler is to approximate this marginal distribution by a typical sample of  $\Psi_{\partial A}$ —typical in the sense of Markov chain sampling.

We introduce the  $R_\lambda[\cdot]$  operation, which acts as

$$R_\lambda : \Psi_{\partial A} \rightarrow \lambda \cdot \Psi_{\lambda^{-1}\partial A}.$$

It maps a state on  $\lambda^{-1}\partial A$  to a state on  $\partial A$  by use of a dilation of parameter  $\lambda > 1$ . For a Gibbs measure endowed with scale invariance, it is shown in Ref. [9] (Sec. II A) that the fixed point of such transformation is a MCMC sampling the infinite plane marginal on  $A$ . The argument is broadly as follows.

(i) We start with any boundary condition  $\Psi_{\partial A}^{\text{gen}}$  (where “gen” stands for generic).

(ii) We construct a chain of iterations of  $R_\lambda$  where  $\lambda > 1$  (in fact, it does not need to be the same on every link):

$$\Psi_{\partial A}^{\text{gen}} \xrightarrow{R_\lambda} R_\lambda[\Psi_{\partial A}^{\text{gen}}] \xrightarrow{R_\lambda} \dots \xrightarrow{R_\lambda} R_\lambda^n[\Psi_{\partial A}^{\text{gen}}] \xrightarrow{R_\lambda} \dots$$

This chain converges to its fixed point, which must be a marginal invariant under rescalings. Reference [9] (Sec. II A) argues that the limit is the distribution obtained when integrating out all fields outside  $A$ , by (1):

$$R_\lambda^n[\Psi_{\partial A}^{\text{gen}}] \rightarrow \Psi_{\partial A} \quad (n \rightarrow \infty).$$

Scale invariance is an essential tool in constructing the marginal distribution.

Using this ingredient, results in Ref. [9] evidenced that finite size and boundary effects could be reduced to negligible levels. This method was dubbed uv sampler as it can be seen as a succession of inverse Kadanoff transformations or a RG flow towards a uv fixed point [12].

## II. ISING 3D UV SAMPLER

*Implemented discrete lattice dilations.* We define  $A$  as a finite volume connected subset of  $\mathbb{R}^3$ , and  $L_A = A \cap \mathbb{Z}^3$  the (square) sublattice contained within. In the implementation choice detailed hereafter,  $A$  is a simple cubic box. When applying a dilation of parameter  $\lambda > 1$ , mapping  $\lambda^{-1}A \rightarrow A$  induces a dilation on the sublattice  $L_{\lambda^{-1}A} \rightarrow L_A$  such that, for<sup>1</sup>  $\sigma_i^L \in \{-1, 1\} \forall \mathbf{i} \in L_A$  the binary lattice variables of the Ising model are mapped as

$$\sigma_{\lfloor \lambda^{-1} \mathbf{i} \rfloor}^L \rightarrow \sigma_{\mathbf{i}}^L, \quad (2)$$

where  $\lfloor \cdot \rfloor$  returns the closest site on  $L_{\lambda^{-1}A}$ . From this point of view, the dilation is not a transformation on  $L_A$  in the sense that the lattice spacing is not dilated but a transformation on the values taken by  $\sigma^L$  on  $L_A$ , i.e., on a configuration  $\bar{\sigma} = \{\sigma_i^L : \mathbf{i} \in L_A\}$ . It is a basic fact of discrete systems that there is more information on  $L_A$  than on  $L_{\lambda^{-1}A}$  meaning that (2) is a one-to-many mapping.

If applying straightforwardly this mapping, a value  $\sigma_i^L$  with  $\mathbf{i} \in \lambda^{-1}A$  could be mapped to many images in  $A$ . This means that a pixel or lump of many identically oriented neighbor sites will be formed. This corresponds to an excess of short distance correlations. It is dubbed a pixel dilation.

In Ref. [9], another prescription was used. First  $L_A$  is partitioned by the equivalence class  $\mathbf{i} \sim \mathbf{j}$  if and only if  $\lfloor \lambda^{-1} \mathbf{i} \rfloor = \lfloor \lambda^{-1} \mathbf{j} \rfloor$ . Second, within each subset of the partition a single site  $\mathbf{i}$  is randomly picked and (2) is performed on it. This forces (2) to be applied in a one-to-one fashion. Last, every unpicked site is unassigned at this stage, in other words left as a hole; a heat-bath procedure is applied on each one of them to assign a spin value depending solely on its first neighbors. Since first neighbors can be missing—either because of being holes themselves, or because they are not in  $A$ —this choice induces a lack of smallest distances ( $\sigma_i \sigma_{i+1}$ ) correlations. This is dubbed heat-bath dilation.

It must be reminded that the rethermalization steps that come after each dilation are performed with fixed boundaries,

fixed  $\sigma_i$  for  $\mathbf{i} \in \partial L_A$ . This has the effect of propagating the new boundary condition inside  $L_A$ . The effects of any dilation prescription only remain on and near the boundary, where the sites will not be updated after discrete dilation.

As a general rule when going 2D to 3D, a larger fraction of the spins are close to the boundary. The direct implication is that the prescription, which was good enough in two dimensions—in Ref. [9]—could leave too strong boundary effects for precision fitting in three dimensions. Anticipating such issues, an hybrid of the pixel and heat-bath prescriptions was implemented. It follows the same partition and second step as heat-bath but in the last stage, on each empty lattice site, at random and with equal probability, either (2) is applied or heat-bath assignment is used. This is named hybrid discrete lattice dilations and has been used in every case throughout this numerical work.

*MCMC description.* The starting point of the MCMC is a  $200 \times 200 \times 200$  cubic Ising lattice in a vacuum ordered state. At zero external magnetic field and normalizing the nearest-neighbour interaction strength  $J$  to 1, the unique coupling is the inverse temperature  $\beta$ , which is set to the estimation<sup>2</sup> of its critical value  $\beta_c$  in Ref. [14]:

$$\beta = \beta_c \approx 0.221\,654\,4 \quad (3).$$

The following steps are taken for the MCMC to produce samples of holographic boundaries.

(i) *Torus intermediate state.* 200 lattice flips, Swendsen-Wang (SW) flips [10], are applied, with periodic boundary conditions. The goal here is to bring the vacuum state to a torus critical state, which is closer to the critical plane, with relatively small CPU effort.

(ii) *Dilations and rethermalizations.* The chain enters then the cycle of hybrid discrete lattice dilations followed by fixed-boundaries SW flips. The parameters—the scaling factor  $\lambda$  and the number  $N_{\text{SW}}$  number of lattice updates—take successive values as per the following lists:

$$\{\lambda\} = \underbrace{2, \dots, 2}_{5 \text{ times}}, \underbrace{1.5, \dots, 1.5}_4, \underbrace{1.3, \dots, 1.3}_4, \underbrace{1.2, \dots, 1.2}_4, \\ \underbrace{1.1, \dots, 1.1}_4, \underbrace{1.05, \dots, 1.05}_7, \underbrace{1.03, \dots, 1.03}_7$$

$$\{N_{\text{SW}}\} = \underbrace{150, \dots, 150}_5, \underbrace{100, \dots, 100}_{16}, \underbrace{80, \dots, 80}_{14}.$$

This means that the first pass is a  $\lambda = 2$  dilation followed by 150 SW flips, this being repeated for the next four passes, etc., until the last pass consisting of a  $\lambda = 1.03$  dilation followed by 80 lattice flips. This totals 35 passes of dilations and lattice flips. At first this can seem like a long process. These somewhat arbitrary numbers give a correctly mixing chain as the following results will show, but this implementation does

<sup>2</sup>It was later pointed to us that Ref. [13] offers the improved numerical estimation  $\beta_c = 0.221\,654\,62$  (2). As a matter of fact, one of the few requirements of the uv sampler is to be provided a coupling value close enough to the critical point to give  $\xi \gg L$ ; this seems verified with our value in use.

<sup>1</sup>Bold variables stand for lattice vectors.

not have any pretension of using the optimal parameters. They were found by trial and error. It takes  $\sim 20$  min to complete this mixing step.<sup>3</sup>

(iii) *Measurements*. This Markov chain measures spatial correlations on the lattice. These correlations involve operators

defined on the lattice: the spin lattice operator  $\sigma_i^L$  and the energy density operator

$$\varepsilon_i^L \equiv \sigma_i^L \sigma_{i+1}^L.$$

The list of measured correlators is explicitly

$$\langle \varepsilon_i^L \rangle, \langle \sigma_i^L \sigma_j^L \rangle, \langle \varepsilon_i^L \varepsilon_j^L \rangle, \langle \varepsilon_i^L \sigma_j^L \sigma_k^L \rangle \text{ and } \langle \varepsilon_i^L \varepsilon_j^L \varepsilon_k^L \rangle.$$

<sup>3</sup>On a single core of an AMD Opteron™ 6174 CPU.

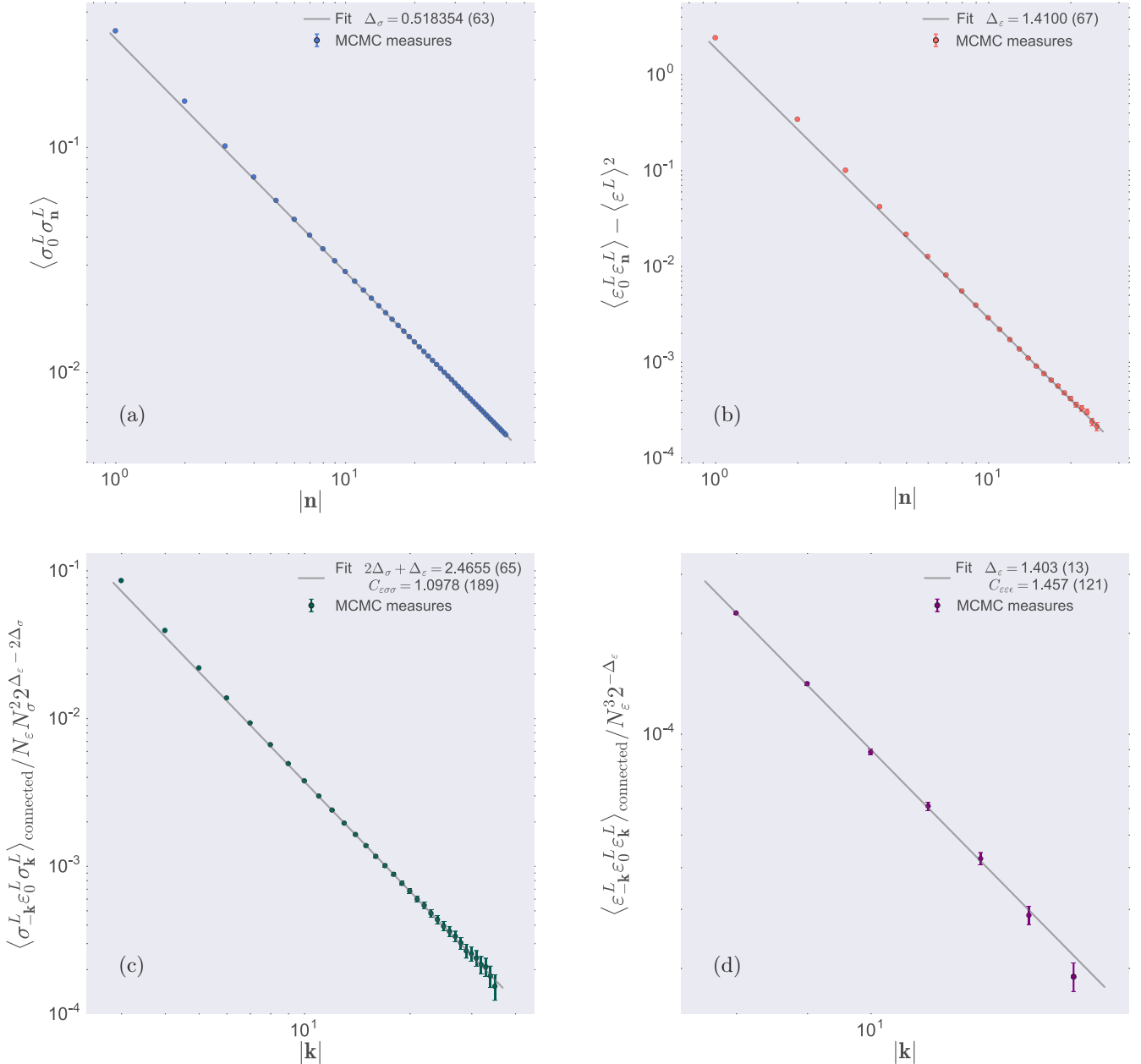


FIG. 1. Measured lattice correlators. (a) Graph of the  $\langle \sigma_0^L \sigma_n^L \rangle$  correlations as a function of the separation  $|n| \in [1, 50]$ . The power-law behavior seems manifest. The gray line represents the most accurate power-law fit. This is solid proof that the sample is very close to the planar expectation. (b) Graph of the  $\langle \varepsilon_0^L \varepsilon_n^L \rangle - \langle \varepsilon^L \rangle^2$  connected two-point function for separations  $|n| \in [1, 25]$ . As much as for  $\sigma^L \sigma^L$  correlations, the power-law behavior is explicit. This observable seems to show more microscopic excess of correlations for the smallest values of the separation. (c) Graph of the connected part  $\langle \sigma_{-k}^L \varepsilon_0^L \sigma_k^L \rangle - \langle \varepsilon^L \rangle \langle \sigma_{-k}^L \sigma_k^L \rangle$  as a function of  $|k| \in [3, 35]$ . With the two  $\sigma^L$  insertions diametrically opposed when sitting on the  $\varepsilon^L$  insertion point, CFT predicts a  $\propto C_{\varepsilon\sigma\sigma} |k|^{-2\Delta_\sigma - \Delta_\varepsilon}$  profile. (d) Graph of the connected part  $\langle \varepsilon_{-k}^L \varepsilon_0^L \varepsilon_k^L \rangle - \langle \varepsilon^L \rangle (\langle \varepsilon_{-k}^L \varepsilon_0^L \rangle + \langle \varepsilon_{-k}^L \varepsilon_k^L \rangle + \langle \varepsilon_0^L \varepsilon_k^L \rangle) - \langle \varepsilon^L \rangle^3$  as a function of  $|k| \in [5, 14]$ . Conformal symmetry constrains the decay to be as  $C_{\varepsilon\varepsilon\varepsilon} N_\varepsilon^3 2^{-\Delta_\varepsilon} |k|^{-3\Delta_\varepsilon}$ .

The long-distance behavior of such correlators is known from their expansion on the basis of the CFT operators:

$$\begin{aligned}\sigma_{\mathbf{i}}^L &= a^{\Delta_\sigma} N_\sigma \sigma(a\mathbf{i}) + \dots, \\ \varepsilon_{\mathbf{i}}^L &= \langle \varepsilon^L \rangle I + a^{\Delta_\varepsilon} N_\varepsilon \varepsilon(a\mathbf{i}) + \dots,\end{aligned}$$

where  $a$  is the lattice spacing, setting  $a = 1$  from here on. This choice of correlators was picked on the principle that they would be enough to fit an interesting subset of the CFT data of the 3D Ising model, namely the scaling dimensions  $\Delta_\sigma$  and  $\Delta_\varepsilon$ , and the three-point couplings  $C_{\varepsilon\sigma\sigma}$  and  $C_{\varepsilon\varepsilon\varepsilon}$ .

Some prescriptions were taken for the insertions choice  $\mathbf{i}$ ,  $\mathbf{j}$ , and  $\mathbf{k}$ : no insertions were made less than 30 lattice units afar from the boundaries—to remove possible remnant boundary effects—and  $\mathbf{i} - \mathbf{j}$ ,  $\mathbf{i} - \mathbf{k}$ , and  $\mathbf{j} - \mathbf{k}$  are always taken along the three lattice directions for computational simplicity. In addition, for the last two correlators listed above, insertions were made with  $\mathbf{j}$  and  $\mathbf{k}$  diametrically opposed when sitting on  $\mathbf{i}$ , e.g.,  $\mathbf{j} - \mathbf{i} = -(\mathbf{k} - \mathbf{i})$ . Each measurement is spaced by five SW flips. Every 20 measurements a new  $\lambda = 1.03$  lattice dilation is applied followed by a rethermalization consisting of 80 SW flips. This aims at updating the boundary configuration and at diminishing the autocorrelations of the measurements [15].

*Uncertainties estimations.* To estimate the uncertainties of the uv sampler is different from estimating the uncertainties of a typical MCMC. Here the relevant quantity measuring the number of uncorrelated samples is not the total number of measurements but the number of boundary configurations used. In the 2D critical Ising model, this is a consequence of exhibiting the property of strong self-averaging, and it has been checked numerically [15]. In our case of interest, the estimation of the uncertainties was done the following way, focusing on the  $\langle \sigma_{\mathbf{0}}^L \sigma_{\mathbf{n}}^L \rangle$  observable.

(i) For each boundary configuration  $\Psi_{\partial A}^i$ , with  $1 \leq i \leq N$ ,  $N \equiv$  total number of boundary states, a graph  $g^i$  of  $\langle \sigma_{\mathbf{0}}^L \sigma_{\mathbf{n}}^L \rangle$  is collected using the operator insertion prescriptions detailed above.

(ii) After having reached the end of the MCMC, we are left with a collection of  $N$  graphs  $S^{\sigma\sigma} = \{g^1, \dots, g^N\}$ . These graphs can be checked to have negligible autocorrelations.  $S^{\sigma\sigma}$  can be read as a matrix with row-index  $|\mathbf{n}|$  and column index  $i$ . The final graph of  $\langle \sigma_{\mathbf{0}}^L \sigma_{\mathbf{n}}^L \rangle$  is obtained by taking a row average over  $S^{\sigma\sigma}$ , and the uncertainty by calculating the standard deviation—along the same direction—and renormalizing it by a  $1/\sqrt{N}$  factor. This is performed for each value of  $|\mathbf{n}|$ .

*Two-point functions and correlators.* Figures 1(a)–1(d) show the results collected for the correlators  $\langle \sigma^L \sigma^L \rangle$ ,  $\langle \varepsilon^L \varepsilon^L \rangle$ ,  $\langle \varepsilon^L \sigma^L \sigma^L \rangle$ , and  $\langle \varepsilon^L \varepsilon^L \varepsilon^L \rangle$ , respectively. The number of samples of  $\Psi_{\partial A}$  used is 9000 for the first two graphs, and 50000 for the last two. For each graph, the axes are log scaled and possible disconnected contributions—from the nonzero one-point expectation value of  $\varepsilon^L$ —were subtracted [16].

The fitted nonuniversal quantities are contained in Table I (Nonuniversal), while universal quantities are split between Table I (Universal) and (Structure constants). All the fits were performed by  $\chi^2$  minimization with each data point weighted by the inverse square of its uncertainty. Details on the fit are stored in Table I (Fit details).

Comments specific to each observable are as follows.

(i)  $\langle \sigma^L \sigma^L \rangle$ , Fig. 1(a): Smallest separations,  $|\mathbf{n}| \leq 5$ , show the most departure from the fitted power law, e.g., fitted on a  $x \rightarrow ax^b$  function,  $a, b$  being the fit's degrees of freedom, this can be imputed to microscopic effects inducing an excess of correlations. The best power-law behavior was fitted for larger separations,  $|\mathbf{n}| \geq 30$ . It is represented on the graph by the gray line.

TABLE I. Summary of the numerical results with comparison to previous MCMCs and CFT bootstrap.

$\langle \varepsilon^L \rangle$	$N_\sigma$	$N_\varepsilon$	
.3302047 (88) <b>.3302022 (5)</b>	Nonuniversal <sup>a</sup> .55245 (13) <b>.550 (4)</b>	.2306 (38) <b>.2377 (9)</b>	
$\Delta_\sigma$		$\Delta_\varepsilon$	
.518354 (63) <b>.5181489 (10)</b>	Universal <sup>b</sup>	1.4100 (67) <b>1.412625 (10)</b>	
$C_{\varepsilon\sigma\sigma}$		$C_{\varepsilon\varepsilon\varepsilon}$	
1.0978 (189) [42] <b>1.051 (3) 1.0518537 (41)</b>	Structure constants <sup>c</sup>	1.46 (12) [2] <b>1.32 (15) 1.532435 (19)</b>	
1.05037 (152) [398] one DOF fit		1.5508 (62) [176] one DOF fit	
Lattice correlator	Function template	Fitting range	$\chi^2$
	Fit details		
$\langle \sigma_{\mathbf{0}}^L \sigma_{\mathbf{k}}^L \rangle$	$x \rightarrow ax^b$	$ \mathbf{k}  \in [30, 50]$	$1.06 \times 10^{-9}$
$\langle \varepsilon_{\mathbf{0}}^L \varepsilon_{\mathbf{k}}^L \rangle_{\text{connected}}$	$x \rightarrow ax^b$	$ \mathbf{k}  \in [10, 25]$	$4.5 \times 10^{-6}$
$\langle \varepsilon_{\mathbf{0}}^L \sigma_{\mathbf{k}}^L \sigma_{\mathbf{k}}^L \rangle_{\text{connected}} / N_\varepsilon N_\sigma^2 2^{\Delta_\varepsilon - 2\Delta_\sigma}$	$x \rightarrow ax^b$	$ \mathbf{k}  \in [12, 35]$	$3.8 \times 10^{-6}$
.	$x \rightarrow ax^{-\Delta_\varepsilon - 2\Delta_\sigma}$	.	$3.8 \times 10^{-6}$
$\langle \varepsilon_{-\mathbf{k}}^L \varepsilon_{\mathbf{0}}^L \varepsilon_{\mathbf{k}}^L \rangle_{\text{connected}} / N_\varepsilon^3 2^{-\Delta_\varepsilon}$	$x \rightarrow ax^b$	$ \mathbf{k}  \in [8, 13]$	$9.6 \times 10^{-8}$
.	$x \rightarrow ax^{-3\Delta_\varepsilon}$	.	$1.02 \times 10^{-7}$

<sup>a</sup>Bold blue entries are the best MCMC estimates found in the literature: respectively, Refs. [13], [18], and [17].

<sup>b</sup>Bold red-color numbers are the numerical bootstrap estimations taken from Ref. [8].

<sup>c</sup>Red numbers are again the numerical bootstrap estimations from Ref. [8], while blue numbers are MCMC results from Ref. [17].

(ii)  $\langle \varepsilon^L \varepsilon^L \rangle$ , Fig. 1(b): To exclude microscopy, the power-law fit was performed on the subset  $|\mathbf{n}| \geq 10$ , after subtraction of the disconnected contribution  $\langle \varepsilon^L \rangle^2$ .

(iii)  $\langle \varepsilon^L \sigma^L \sigma^L \rangle$ , Fig. 1(c): After removal of the disconnected contribution, a power-law fit for insertions  $|\mathbf{n}| \in [12, 35]$  returns exponent and offset estimates agreeing with the bootstrap predictions. In particular the fitted structure constant 1.0978(189) has a satisfying agreement. In estimating the structure constant by fitting the offset of this correlator, it is necessary to remove the  $N_\sigma^2 N_\varepsilon$  contribution by using our estimates of  $N_\sigma$  and  $N_\varepsilon$  from the previous two correlators estimations, see Table I (Nonuniversal) for values. The systematic error from the uncertainty of  $N_\sigma$  is negligible, unlike the (larger relative) uncertainty of  $N_\varepsilon$ . To minimize this error the more precise value from Ref. [17]— $N_\varepsilon = .2377(9)$ —is used. This gives a systematic error contribution of  $4.2 \times 10^{-3}$ , written in square brackets in Table I (Structure constants).

For a numerical estimation with smaller uncertainty, one option is to remove  $\Delta_\sigma$  and  $\Delta_\varepsilon$  from the fit free parameters by replacing them by their bootstrap estimations. Such fit with a single degree of freedom (DOF), and performed on the same range, returns  $C_{\varepsilon\sigma\sigma} = 1.05037(152)$  [398]. This result is in striking agreement with the bootstrap estimation.

(iv)  $\langle \varepsilon^L \varepsilon^L \varepsilon^L \rangle$ , Fig. 1(d): Here again, nonconnected contributions need to be removed to reveal an approximate power-law profile. Fitting on a power law and reading the exponent gives a close estimate of the energy density scaling weight at 1.403(13). The offset fit offers a  $C_{\varepsilon\varepsilon\varepsilon}$  numerical estimation of 1.46(12) [2] for a fitting range  $|\mathbf{k}| \in [8, 13]$ . This fitting uncertainty is rather large, but the estimate is in a  $1\sigma$  range of the CFT bootstrap value.

If restricting the fit to a single degree of freedom, its offset, by inputting the bootstrap value of  $\Delta_\varepsilon$  and fitting on  $x \rightarrow$

$ax^{-3\Delta_\varepsilon}$ , our estimation becomes 1.5508(62) [176]. The latter fit is in much closer agreement with the expected value. In the single DOF fits of the two structure constants, the main contribution to the error comes from the uncertainty on  $N_\varepsilon$  and a more accurate numerical estimation of each constant would require a more precise knowledge of  $N_\varepsilon$ .

### III. DISCUSSION

The general conclusion is that the averages show a behavior close to their expectation on the infinite plane. Especially the measurements of the  $\langle \sigma_i^L \sigma_j^L \rangle$  and  $\langle \varepsilon_i^L \varepsilon_j^L \rangle_{\text{connected}}$  show clear power-law profiles typical of planar CFTs. In addition, the fitted nonuniversal and universal observables match with previous Monte Carlo studies [17, 18], which use an entirely different method based on a massive deformation of the CFT to reduce their finite-size and boundary effects, and agree within smaller uncertainties with the more precise bootstrap methods [5], see Table I (Weights) and Table I (Structure constants).

Further work could include the study of the complete profile of  $\langle \varepsilon_i^L \sigma_j^L \sigma_k^L \rangle_{\text{connected}}$  as its CFT formula depends on the assumption that conformal invariance follows from scaling invariance in dimensions. The investigation of four-point functions such as  $\langle \sigma_i^L \sigma_j^L \sigma_k^L \sigma_l^L \rangle$  could also bring numerical insights on its expansion on conformal blocks [6].

### ACKNOWLEDGMENTS

The author would like to express gratitude to B. Doyon for his guidance and numerous advice. The author is funded by a Graduate Teaching Assistantship from KCL Department of Mathematics.

---

[1] R. Peierls, On Ising’s model of ferromagnetism, in *Mathematical Proceedings of the Cambridge Philosophical Society* (Cambridge University Press, Cambridge, 1936), Vol. 32, pp. 477–481.

[2] L. Onsager, Crystal statistics. I. a two-dimensional model with an order-disorder transition, *Phys. Rev.* **65**, 117 (1944).

[3] L. D. Landau and V. L. Ginzburg, On the theory of superconductivity, *Zh. Eksp. Teor. Fiz.* **20**, 1064 (1950), also republished in *On Superconductivity and Superfluidity* (Springer, Berlin, Heidelberg, 2009).

[4] S. El-Showk, M. F. Paulos, D. Poland, S. Rychkov, D. Simmons-Duffin, and A. Vichi, Solving the 3D Ising model with the conformal bootstrap, *Phys. Rev. D* **86**, 025022 (2012).

[5] F. Kos, D. Poland, D. Simmons-Duffin, and A. Vichi, Precision islands in the Ising and  $O(N)$  models, *J. High Energy Phys.* **08** (2016) 036.

[6] D. Simmons-Duffin, The conformal bootstrap, in *New Frontiers in Fields and Strings (TASI 2015)-Proceedings of the 2015 Theoretical Advanced Study Institute in Elementary Particle Physics*, edited by J. Polchinski *et al.* (World Scientific Publishing Co. Pte. Ltd., Singapore, 2017), pp. 1–74.

[7] D. Poland and D. Simmons-Duffin, The conformal bootstrap, *Nature Phys.*, **535** (2016).

[8] D. Simmons-Duffin, The lightcone bootstrap and the spectrum of the 3D Ising CFT, *J. High Energy Phys.* **03** (2017) 086.

[9] V. Herdeiro and B. Doyon, Monte carlo method for critical systems in infinite volume: The planar Ising model, *Phys. Rev. E* **94**, 043322 (2016).

[10] R. H. Swendsen and J. Wang, Nonuniversal Critical Dynamics in Monte Carlo Simulations, *Phys. Rev. Lett.* **58**, 86 (1987).

[11] V. Herdeiro, Markov chain sampling of the  $O(n)$  loop models on the infinite plane, *Phys. Rev. E* **96**, 013305 (2017).

[12] V. Herdeiro and B. Doyon (unpublished).

[13] M. Hasenbusch, Thermodynamic Casimir effect: Universality and corrections to scaling, *Phys. Rev. B* **85**, 174421 (2012).

[14] A. Talapov and H. W. J. Blöte, The magnetization of the 3D Ising model, *J. Phys. A: Math. Gen.* **29**, 5727 (1996).

[15] V. Herdeiro (unpublished).

[16] See Supplemental Material at <http://link.aps.org/supplemental/10.1103/PhysRevE.96.033301> for numerical values of these data points.

[17] G. Costagliola, Operator product expansion coefficients of the 3D Ising model with a trapping potential, *Phys. Rev. D* **93**, 066008 (2016).

[18] M. Caselle, G. Costagliola, and N. Magnoli, Numerical determination of the operator-product-expansion coefficients in the 3D Ising model from off-critical correlators, *Phys. Rev. D* **91**, 061901 (2015).